RSC Advances

PAPER

View Article Online
View Journal | View Issue

Cite this: *RSC Adv.*, 2021, **11**, 18590

Mineralization of calcium phosphate induced by a silk fibroin film under different biological conditions†

Ying Huang,‡[a] Zhaoyong Zou,‡[a] Hang Ping,[a] Liwen Lei,[a] Jingjing Xie,[a] Hao Xie*[b] and Zhengyi Fu*[a]

Received 19th March 2021
Accepted 10th May 2021

DOI: 10.1039/d1ra02199k

rsc.li/rsc-advances

Silk fibroin is a promising biomaterial that has been used for tissue engineering applications. However, the influence of silk fibroin on the mineralization of calcium phosphate in different biological environments has not been discussed before. In this work, we fabricated organized silk fibroin film as the organic framework and amorphous calcium phosphate (ACP) deposited on the films as precursors. The transformation pathways and morphology of ACP was then studied in both enzyme and PBS (phosphate buffer saline) solutions. While only hydroxyapatite (HA) crystals formed in enzyme solution, a mixture of tricalcium phosphate (TCP) and HA crystals were obtained in PBS solution, which can be related to the variations of the content of silk fibroin and pH of the solution. Therefore, silk fibroin films can have an important effect on the mineralization process of calcium phosphate in different biological environments. In addition, cell cultivation experiments show that the silk films after mineralization promoted osteogenesis and exhibited good biocompatibility.

Introduction

Over billions of years of evolution, biological systems have been able to construct unique structures with superior properties at ambient temperature, which provides them with special functions for adapting to the environment.[1] Studying the formation process of biological structures provides inspirations for the novel synthesis and processing of materials. Based on this idea, the concept "bioprocess-inspired fabrication" has been recently proposed.[2]

Bone is a typical example of biological composites, which mainly consists inorganic hydroxyapatite (HA) nanocrystals and organic macromolecules such as collagen, glycoproteins and proteoglycans.[3] The hierarchical organization over multiple length scales provides the bone good mechanical properties, such as high fracture toughness and high strength.[4–6] Owing to the increasing clinical requirements for promoting bone regeneration, many scaffold materials have been developed, which are mainly collagen-based composite scaffolds. However, the manufacturing cost to obtain collagen molecules from natural resources is very high and the collagen-based scaffolds are generally poor at mechanical performance as the load bearing structure in bone repairing.[7] Scientists alternatively explored other natural materials such as silk fibroin, chitosan, alginate, cellulose as well as synthetic materials such as poly(glycolic acid) (PGA), poly(lactic acid) (PLA) and polycaprolactone (PCL) as frameworks to mediate the formation of inorganic crystals.[5,8–10] Silk fibroin is a fibrous protein with nanostructures similar to that of collagen, and has been extensively investigated as an alternative polymer of collagen.[11] Silk fibroin can be dissolved and form regenerated silk materials through acid treatment. Morphology, mechanical and biological properties of regenerated silk materials can be controlled by acidic and ionic solutions.[12,13] The silk-based materials can then be used as the templates to induce nucleation and growth of apatite. They can also form a tougher and stronger structure than that of collagen-based ones.[14] Yet, it remains difficult to precisely control the morphology and structural organization of inorganic crystals using silk fibroin solution or silk scaffolds.

The general process of bone formation includes (i) secretion of extracellular matrix with certain degree of organization, (ii) formation of amorphous calcium phosphate (ACP) within the matrix under the regulation of non-collagenous proteins, and (ii) transformation of ACP into HA crystals along the long axis of collagen fibrils.[15–18] Adopting the formation principle of bone will facilitate the synthesis of bone-biomimetic composites and provide alternatives of traditional bone grafts.[19,20] Martin and co-workers[15] explored the formation of highly oriented scaffold with self-assembled liquid crystal Pluronic F127. However, it is

[a]State Key Laboratory of Advanced Technology for Materials Synthesis and Processing, Wuhan University of Technology, Wuhan, 430070, China. E-mail: zyfu@whut.edu.cn
[b]School of Chemistry, Chemical Engineering and Life Science, Wuhan University of Technology, Wuhan, 430070, China. E-mail: h.xie@whut.edu.cn

† Electronic supplementary information (ESI) available. See DOI: 10.1039/d1ra02199k

‡ These authors contributed equally to this work.

not easy to control the alignment of the polymers due to their sensitivity to harsh processing conditions.

In this study, instead of using silk fibroin solution or silk scaffolds, we propose to use organized silk fibroin film to induce the mineralization of calcium phosphate. Silk films were prepared and immersed in simulated body fluids (SBF) to induce the formation of ACP. The films were then incubated in three different environments including protease solution, PBS solution and cell seeded environment. Results show that the transformation pathways of ACP and morphologies of calcium phosphate crystals varied in different environments. In addition, the biological properties of the prepared films were investigated. These results are useful for application of silk fibroin films in bone tissue engineering.

Experimental

Preparation of silk fibroin films (SF)

Degummed silk was purchased from Simatech Incorporation (Suzhou, China) and dissolved in 5 wt% $CaCl_2$–formic acid (FA) with different concentrations. After three hours of vigorous stirring, SF were generated by evaporating silk fibroin solutions and then immersed in deionized water for 12 hours. The SF were cut into round pieces with diameters of 10 mm for subsequent study.

SF induced mineralization

Mineralization of calcium phosphate induced by SF was performed at ambient temperature (~15 °C) by immersing the film in 10× SBF solution (1 M NaCl, 5 mM KCl, 25 mM $CaCl_2 \cdot 2H_2O$, 5 mM $MgCl_2 \cdot 6H_2O$, 3.62 mM Na_2HPO_4, 10 mM $NaHCO_3$) under agitation for 24 hours.[21] The obtained SF after mineralization (MSF) were washed three times with deionized water and immediately cooled at −70 °C for 2 hours, followed by vacuum drying for 24 hours.

Characterization of SF and MSF

Surface morphology and cross profile of SF and MSF were characterized by a field emission scanning electron microscope (FESEM, Hitachi, S-4800) at 5 kV. All samples were fixed on a carbon tape and sputter coated with platinum before imaging.

Fourier transform infrared (FTIR) spectra were acquired by using a Thermo Scientific Nicolet 6700. Samples were grinded with potassium bromide powder and pressed into slices. FTIR spectra were collected in the region of 4000–400 cm^{-1}. All samples were scanned 32 times with a resolution of 4 cm^{-1}.

X-ray diffraction (XRD) of SF and MSF were performed by using a Bruker D8 Advance, with Cu Kα radiation (40 kV, 40 mA). XRD patterns were recorded at a 2θ range of 15°–100° for 30 minutes.

Thermogravimetric (TG) analysis of SF and MSF was performed using a Discovery TGA (TA Instruments). TG measurements were carried out in nitrogen atmosphere with a temperature range of 40–1000 °C at a heating rate of 10 °C min^{-1}.

Swelling ratio was analysed by immersion SF and MSF in PBS at 37 °C to complete swelling and obtain the wet weight (W_{wet}). After vacuum drying, the weight of all samples was recorded as dry weight as (W_{dry}). Swelling ratio was calculated by using the following formula.

$$\text{Swelling ratio\% } (Q) = (W_{wet} - W_{dry})/W_{dry} \times 100$$

Silk fibroin films were cut into rectangle pieces (0.5 × 3 cm) and subjected to mechanical tests by measuring the tension on a universal testing machine (MTS, CMT 5105) at 25 °C, with the humidity of 65%, and at a testing rate of 1.0 mm min^{-1}.

Contact angle of SF and MSF were measured by a contact angle meter (DataPhysics OCA 35, Germany).

Degradation and mineralization in enzyme and PBS solution

The degradation and mineralization of SF and MSF were performed in both enzyme and PBS solution. The enzyme solution was prepared by dissolving 3.5 units per mg of protease (Sigma, Cat Number: P5417-1G, Japan) in PBS solution. Dry weight of SF before immersion was recorded. The degradation experiments were performed by adding 1 piece of SF with a diameter of 10 mm into 1 mL enzyme or PBS solution and incubated at 37 °C for 2–24 hours. The weight of each sample ranges from 0.008 to 0.048 g for 3–15% SF and 0.011–0.055 g for 3–15% MSF, respectively. After incubation, samples were then taken out of the solution and washed three times with distilled H_2O. After vacuum drying, the weight of the samples was recorded before characterization. Samples were also treated with PBS for 40 days. The pH change of the solution was measured during both experiments. The crystal transformation in PBS and enzyme solutions were detected by SEM, XRD, transmission electron microscopy (TEM) equipped with energy-dispersive X-ray spectroscopy (EDS) (Talos F200S, Thermo Scientific, United States).

Cell cultivation on SF and MSF

Osteoblast cells were purchased from Procell Life Science & Technology Co., Ltd. (Wuhan, China) and cultured at 37 °C, 5% CO_2, in Dulbecco's modified Eagle's medium (DMEM, Gibico), supplied with 10% (v/v) FBS (fetal bovine serum, Gibico, USA), 1% PS (v/v) (penicillin–streptomycin, Sigma, USA) as well as 1% (v/v) L-glutamine. Passage 4 cells were used for all experiments.

SF and MSF were exposed to UV-light for 30 minutes, and then soaked in 75% ethanol for 2 hours. After rinsing with PBS twice, the films were immersed in culture media overnight before cell seeding. Cells at the number of 2×10^4 were seeded on each film.

Cell morphology was imaged with an optical microscopy (Mshot, MS60) and SEM. For SEM observation, cells were fixed in 2.5% glutaraldehyde at 4 °C for 4 hours and dehydrated with graded ethanol (30%, 50%, 70%, 85% and 90%). Samples were then vacuum dried and sputter coated with platinum.

Proliferation and viability of osteoblast cultured on SF and MSF were measured with Cell Counting Kit-8 (CCK-8, Sangon Biotech, China). Cells were incubated in culture media along

with CCK-8 solution at a ratio of 1 : 10. The absorbance of formazan was recorded at 450 nm on a microplate reader (BioTek, USA).

Alkaline phosphatase (ALP) activity of osteoblasts showed cell differentiation on SF and MSF. Samples were washed twice with PBS and treated with ALP staining kit (Solarbio, China). Stained samples were imaged with an optical microscope.

Calcium deposition induced by cells was measured by using Alizarin Red-sulfate staining kit (Solarbio, China). Samples were fixed with 95% ethanol, washed with PBS, and stained for 3 minutes. Stained samples were photographed with an optical microscope.

Statistics

All data were from triplicate measurements and reported as mean ± standard deviation. One way ANOVA tests were performed for statistical analysis.

Results and discussion

Fabrication and characterization of MSF

SF were obtained by dissolving 3 wt% to 15 wt% silk fibroins in FA–$CaCl_2$ solution and subsequent fast evaporation of FA,[22] which facilitated self-assembly of silk fibroin nanofibers into thin film. The thickness of the film increases from 0.32 to 1.03 mm with increasing concentration of dissolved silk fibroins from 3 wt% to 15 wt% (Table S1†). SEM images show that the morphology of SF obtained from different silk fibroin concentrations was similar (Fig. S1†). It is clear that the film was assembled by oriented silk nanofibers and there is a significant amount of nanopores in the film (Fig. 1A and B). Mineralization of calcium phosphate induced by SF was initiated by incubating the film in 10× SBF solution at ambient temperature for 24 hours. The stability of ACP strongly depends on the environmental conditions. The 10× SBF we used in this study, which is a supersaturated solution and may be beneficial to the stability of ACP.[23,24] As shown in Fig. 1C and D, spherical nanoparticles of about 50–100 nm precipitated on the surface of SF and grew along silk nanofibers. Most of the nanoparticles were found on the surface and some also existed within the interior of the SF. TG results (Fig. S2†) show similar weight loss between the SF and MSF, suggesting that the mineral content is very low as compared to the organic silk fibroin in SF. The hydrophilicity/hydrophobicity of the SF/MSF was evaluated by contact angle measurement. Results (Fig. S3†) show that the contact angle of SF and MSF is 112.4° and 71.6°, respectively. It suggests that the mineralization increases the hydrophilicity of silk fibroin film, which is important for the biocompatibility of MSF.[5] The influence of mineralization on pore size and porosity of silk fibroin films was investigated by determining the swelling ratio of the SF and MSF, where a higher swelling ratio indicates a higher water retaining ability and a higher porosity. Results (Fig. S4†) show that the swelling ratio of silk fibroin films decrease after mineralization for SF prepared at all concentrations of silk fibroin, suggesting that mineralization reduces the porosity of the silk film. Mechanical tests showed that mineralization process could reduce the tensile strength of the SF (Fig. S5†). Since the mineralization results of SF with different concentrations are similar, data of the sample with 15 wt% silk fibroins will be represented in the following part unless specifically noted.

SF before and after mineralization were subjected to FTIR and XRD analysis (Fig. 2). The peaks at 1654, 1519 and 1235 cm^{-1} were detected in the FTIR spectra of both SF and MSF (Fig. 2A), which can be attributed to the amide I, amide II and amide III bands of silk fibroin, respectively.[5,25,26] The similar positions of these peaks suggest that the secondary structure of silk fibroin did not change after mineralization. In addition, the spectrum of the MSF shows two prominent bands at 563 cm^{-1} and 1058 cm^{-1}, which corresponds to the ν_3 and ν_4 vibrations of phosphate, respectively. The position of these two peaks suggests that the mineral phase was ACP.[23] The XRD pattern of SF (Fig. 2B) show a broad peak at 20° (2θ), which could be attributed to the β-sheet structure of silk fibroin.[27] In MSF, the pattern show an additional hump at 30°, which further confirmed that the minerals were amorphous calcium phosphate.[23]

Mineral transformation in biological environment

The degradation of biomaterials in human body is often induced by enzymes. To mimic the transformation from ACP to crystalline calcium phosphate *in vivo*, PBS and enzyme solutions were used to initiated the transformation. The enzyme

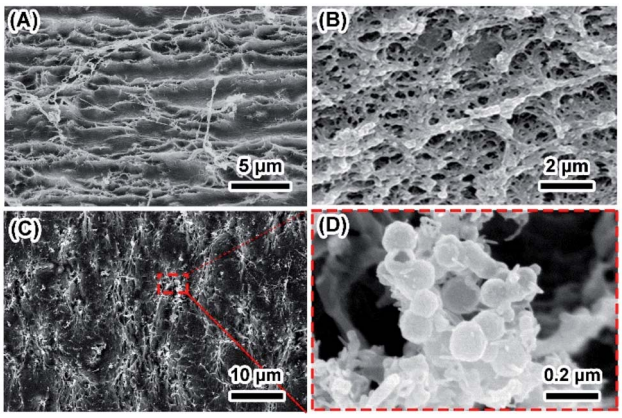

Fig. 1 Typical morphology of SF and MSF. Panels (A and B) show the surface and cross section of SF. Panels (C and D) show the low and high magnification image of the surface of MSF.

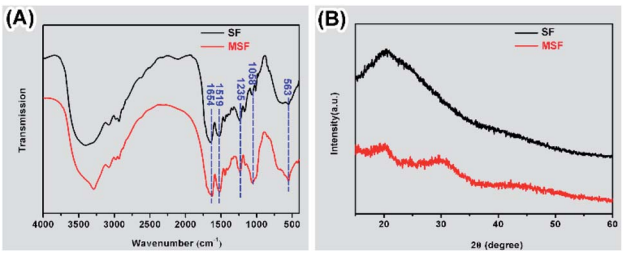

Fig. 2 (A) FTIR spectra, (B) XRD patterns of SF and MSF.

solution in this work can partially mimetic the biological environment and the PBS solution treatment is the control group. In enzyme solution (Fig. 3A), ACP transforms to HA after 2 hours, where the XRD data show the a appearance of peaks at 25°, 31.5° and 32°, which correspond to (002), (211) and (112) plane of HA (PDF#82-1943), respectively.[23] In addition, the intensity of the peaks increased with time, suggesting an increasing amount of crystals. In PBS solution (Fig. 3B), the mineral was confirmed to be the mixture of $Ca_3(PO_4)_2$ (TCP) (PDF#89-8960) and HA by XRD.[28] Similarly, the intensity of peaks at 30.1° (102) (TCP) and 32° (112) (HA) became stronger after 24 hours PBS immersion. These results imply that the crystallization pathway of ACP in enzyme solution and in PBS solution were different. While only HA forms in enzyme solution, a mixture of TCP and HA forms in PBS solution.

The morphology of minerals during crystallization was also investigated. SEM images show that spherical ACP nanoparticles gradually transformed into thin sheet-like structure after soaking in enzyme solution and large plate-like crystals were observed after 12 hours (Fig. 4, panels A, B1–B4). For transformation in PBS solution (Fig. 4, panels A, C1–C4), the morphological change in the early stage is similar, but no large plate-like crystals can be observed after 24 hours. The morphology of the sample in enzyme solution was further investigated by TEM and SAED. TEM image show that after 2 hours the thin sheet-like structures were mainly attaching on the surface of the spherical nanoparticles. However, no sharp diffraction rings or spots could be observed from the corresponding SAED pattern (Fig. 4, panels D and E), suggesting that the sample was mainly amorphous. Although the sheet-like structure may be crystallized, such a small amount would be difficult to be detected by SAED. After 24 hours, no spherical nanoparticles could be observed and all nanoparticles have transformed into sheet-like structure. SAED pattern of the sample show two strong diffraction rings, which could be ascribed to the (211) and (002) reflection of hydroxyapatite[29] (Fig. 4, panels F and G). EDS results (Table S2†) showed that the Ca/P ratio in enzyme solution is 1.57 ± 0.07, which corresponds to the Ca/P ratio of HA ranging from 1.50 to 1.67.[30] These data are consistent with the XRD results (Fig. 3A).

To further analyse the influence of incubating solution on the samples, we detected the change of scaffold weight and pH

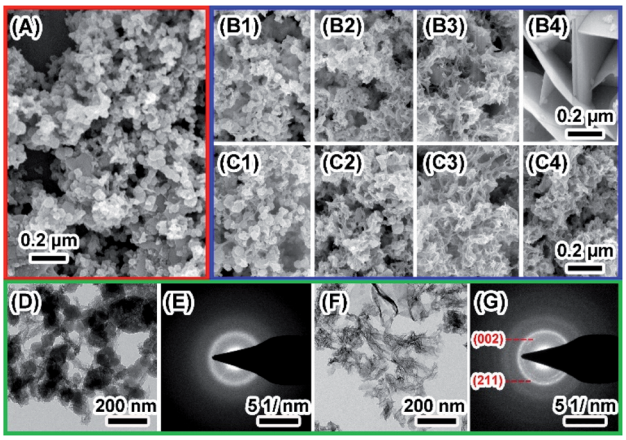

Fig. 4 Changes of morphology and crystallization of ACP induced in enzyme and PBS solution. Panel (A) shows SEM of ACP formed in 10× SBF. Panels (B1–B4) show SEM of ACP after soaking in enzyme solutions for 2, 6, 12 and 24 hours. Panels (C1–C4) show SEM of ACP after soaking in PBS solutions for 2, 6, 12 and 24 hours. Panels (D and E) show TEM and SAED of ACP after soaking in enzyme solutions for 2 hours. Panels (F and G) TEM and SAED for ACP after soaking in enzyme solutions for 24 hours.

variations of the solutions. Upon enzymatic digestion, weight loss was observed for both SF and MSF (Fig. 5A). SF obtained at higher concentrations of silk fibroins exhibited lower ratio of weight loss than those obtained at lower concentrations of silk fibroins. At the beginning of enzymatic digestion, both SF and MSF showed similar trends of weight loss. While at the end of enzymatic digestion, SF generally exhibited higher depredating ratio than that of MSF, implying minerals on silk fibroins may provide protection against enzymatic digestion. However, trends were different in PBS solutions (Fig. 5B). MSF showed significantly higher weight loss ratio than unmineralized

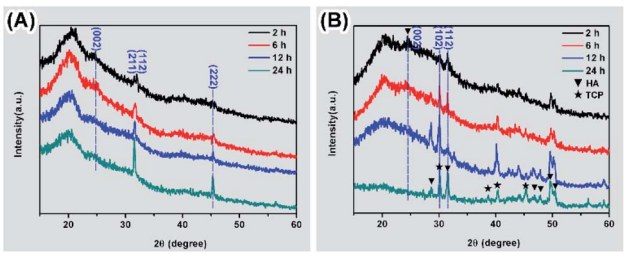

Fig. 3 Changes of XRD of MSF induced in enzyme and PBS solution. Panel (A) shows XRD of ACP after soaking in enzyme solutions for 2, 6, 12 and 24 hours; panel (B) shows XRD of ACP after soaking in PBS solutions for 2, 6, 12 and 24 hours.

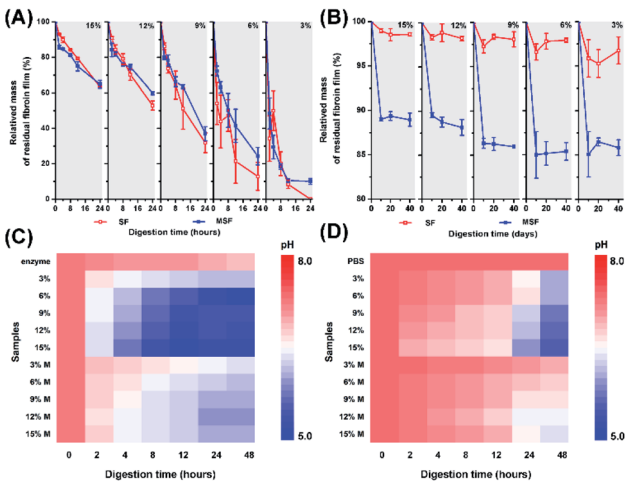

Fig. 5 Weight loss of MSF and SF and the pH change of solution treated by enzyme (A, C) and PBS (B, D) solutions. Panels (A, B) show weight depletion of enzymatic and PBS degradation of MSF and SF formed in different concentrations of silk fibroin; panels (C, D) show pH changes during enzymatic and PBS treatment of MSF and SF.

samples in 40 days. In general, SF in PBS solutions were relatively stable than that in enzyme solution and the total weight loss were less than 5% for all samples. It can also be observed that the weight loss decreased slightly for SF with higher concentrations, while the weight loss of MSF was higher than 10%. Therefore, the significantly higher weight loss for MSF as compared to SF in PBS solution is most likely originated from the transformation of ACP minerals.

During immersion of SF and MSF in enzyme and PBS solution, the pH of both solutions decreased (Fig. 5C and D). Compared with MSF, degradation of SF led to lower pH. In addition, the pH of enzyme solutions was lower than that of PBS solutions after immersion of the films. These may due to the higher degradation ratio of SF in enzyme solution and the release of amino acids from silk fibroins. At low pH, Ca^{2+} can stably bind to the hydrophobic chains of silk fibroin. The β-sheet structure in hydrophobic chains is able to regulate the formation of hydroxyapatite.[27,31] Taking these observations together, the different transformation pathways of ACP may be related to variation of silk fibroin content and pH value in PBS and enzyme solutions. The degradation of silk fibroin in enzyme solution is faster than that in PBS solution, which leads to a higher amount of amino acid and a lower pH of the solution, as shown in Fig. 5. Previous studies have shown that the pH of the solution has a strong influence on the transformation of ACP. In addition, the presence of organic molecules could also affect the crystallization pathways of ACP.[23]

Cell cultivation and mineralization on silk films

To explore the biocompatibility of silk fibroin films as scaffold for bone tissue engineering and the influence of cell culture on ACP transformation, osteoblasts were cultured on both SF and MSF. Attachment of round shape osteoblasts to the surface only occurred in 15% SF after one day of cultivation (Fig. 6A) and some cells were observed expanding on silk film surface in all other samples (Fig. 6B). Morphological difference of mineral was also observed on MSF where osteoblasts grew. Flower like mineral aggregations were observed on MSF formed in both 15% and 12% SF (Fig. 6C and D), which were significantly different from the minerals observed in enzyme solution and PBS solution. The phase transformation of ACP in cell culture environment was investigated by XRD analysis (Fig. 7). The characteristic peaks of hydroxyapatite at 25.8° and 31.6° were already detected after cell cultivation for 4 hours.[23] The increasing intensity of diffraction peaks suggests a gradual transformation from ACP to hydroxyapatite.

Factors affecting ACP transformation and biocompatibility of MSF were evaluated by means of CCK8, ALP and red-sulfate staining met hod. CCK8 results showed fast cell growth on both SF and MSF within 5 days and the growth rate slowed down or cell apoptosis occurred in day 7 (Fig. 8A and B). ALP is a marker for osteogenic formation as it plays important roles in osteogenic development.[9] Higher ALP activity of osteoblasts on MSF was observed than that on SF (Fig. 8C–E and S2†), indicating that MSF promoted osteogenesis. Red-sulfate is a dye that can be used to examine the deposition of red-stained calcium nodular (Fig. 8F–H and S2†).[32] Higher density of calcium was observed on MSF than that on SF, suggesting that mineralized films also promoted osteoblasts calcium deposition.

For the formation of minerals on MSF under cell culture condition, th e cell culture media contains DMEM, FBS, and L-glutamine *etc.*, which were not present in enzyme solution and PBS solution. In addition, osteoblasts attached on the surface of the MSF could secrete a significant amount of extracellular matrix. All these factors could dramatically influence the crystallization pathway of ACP.[33]

In brief, cell differentiation, cell proliferation and metabolites produced by cells may affect the environment of culture media and influence the transformation of ACP. It is also concluded that MSF have good potential in bone tissue engineering due to the good biocompatibility of MSF to osteoblasts

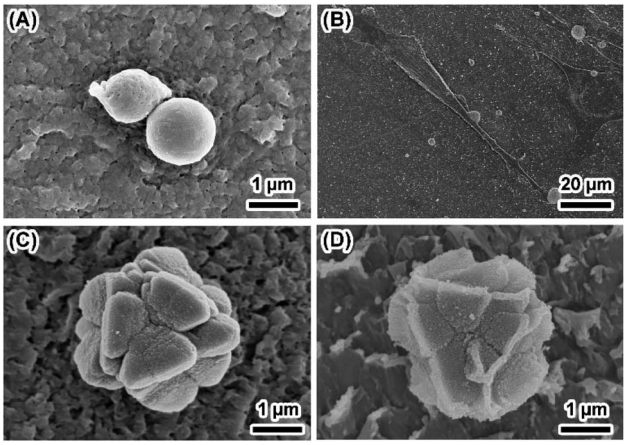

Fig. 6 Cultivation of osteoblasts on SF and MSF. Panels (A–C) show SEM image of osteoblast after 1 day of cultivation on SF obtained in (A) 15%, (B) 12% silk fibroins. Panel (C and D) shows SEM image of mineral morphology after 1 day of cultivation on MSF obtained in 15% and 12% silk fibroins.

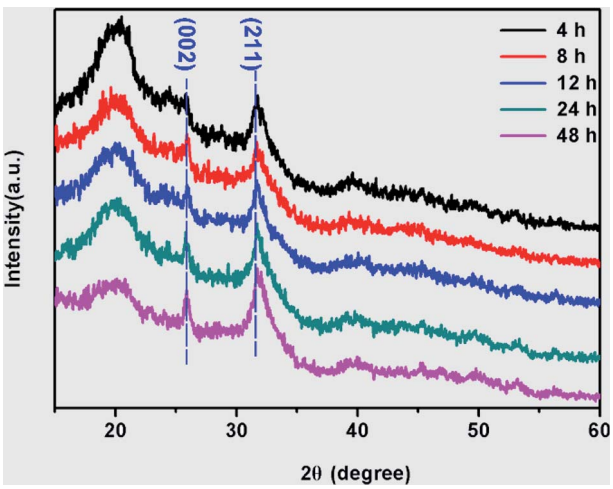

Fig. 7 XRD of MSF after cell culture for 4, 8, 12, 24 and 48 hours.

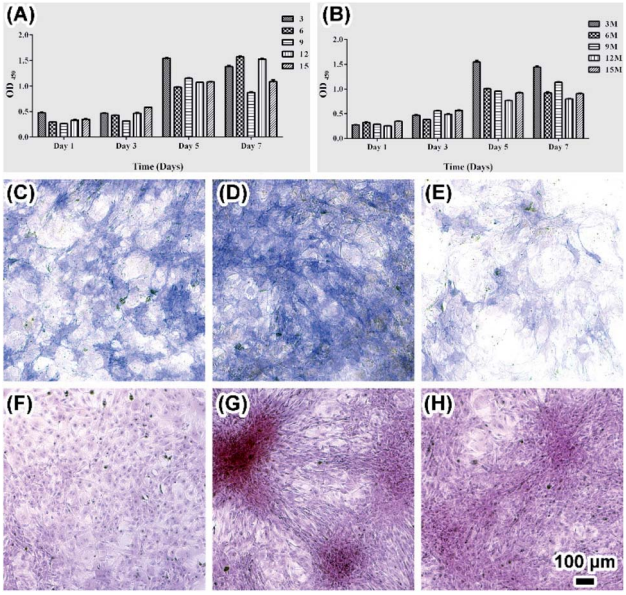

Fig. 8 CCK8 assessments of cells cultured on (A) SF and (B) MSF; ALP staining and red sulfate staining of osteoblast cultivation with or without silk fibroin films. Panels (C–E) show ALP staining of osteoblast cultivation on (C) SF, (D) MSF, or (E) without films. Panels (F–H) show red sulfate staining of osteoblast cultivation on (F) SF, (G) MSF, or (H) without films.

as well as the ability of MSF in promoting osteogeneses and mineralization.

Conclusions

The silk fibroin films framework composed of oriented nanofibers was used to induce the mineralization of apatite crystals. We first obtained the formation of ACP nanoparticles along silk nanofibers after immersing the films in SBF solution. The transformation from ACP into hydroxyapatite was achieved in PBS and enzyme solution, in which the transformation patterns were different. These results are useful to understand the progress of hydroxyapatite formation in biological environments. Mineralized silk fibroin films promoted osteogeneses and exhibited good biocompatibility. The present study promotes the understanding of apatite crystallization within the framework of silk film and contributes to the fabrication of bone mimetic materials that are promising in bone tissue engineering.

Conflicts of interest

There are no conflicts to declare.

Acknowledgements

National Natural Science Foundation of China (31771032, 51521001, 51832003, 51911530153).

Notes and references

1 C. Pang, T.-i. Kim, W. G. Bae, D. Kang and M. K. Sang, *Adv. Mater.*, 2012, **24**, 475–479.
2 J. Xie, H. Ping, T. Tan, L. Lei, H. Xie, X.-Y. Yang and Z. Fu, *Prog. Mater. Sci.*, 2019, **105**, 100571.
3 C. Li, J. Hu, J. Ran, X. Shen and T. Hua, *Polym. Compos.*, 2014, **37**, 81–90.
4 E. A. Zimmermann and R. O. Ritchie, *Proc. Natl. Acad. Sci. U. S. A.*, 2011, **108**, 14416.
5 Y. Gao, W. Shao, W. Qian, J. He, Y. Zhou, K. Qi, L. Wang, S. Cui and R. Wang, *Mater. Sci. Eng., C*, 2018, **84**, 195–207.
6 J. Y. Rho, L. Kuhn-Spearing and P. Zioupos, *J. Biomed. Eng.*, 1998, **20**, 92.
7 M. Yang, W. He, Y. Shuai, S. Min and L. Zhu, *J. Polym. Sci., Part B: Polym. Phys.*, 2013, **51**, 742–748.
8 S. Aday and M. e. Gümüşderelioğlu, *Polym. Compos.*, 2010, **31**(8), 1418–1426.
9 D. Su, L. Jiang, X. Chen, J. Dong and Z. Shao, *ACS Appl. Mater. Interfaces*, 2016, **8**, 9619–9628.
10 M. B. Stewart, S. R. Gray, T. Vasiljevic and J. D. Orbell, *Carbohydr. Polym.*, 2014, **102**, 246–253.
11 J. Wang, W. Zhou, W. Hu, L. Zhou, S. Wang and S. Zhang, *J. Biomed. Mater. Res., Part A*, 2011, **99**, 327–334.
12 J. Ming, Z. Liu, S. Bie, F. Zhang and B. Zuo, *Mater. Sci. Eng., C*, 2014, **37**, 48–53.
13 G. S. Perrone, G. G. Leisk, T. J. Lo, J. E. Moreau, D. S. Haas, B. J. Papenburg, E. B. Golden, B. P. Partlow, S. E. Fox and A. M. Ibrahim, *Nat. Commun.*, 2014, **5**, 3385.
14 J. Wang, G. Yang, Y. Wang, Y. Du, H. Liu, Y. Zhu, C. Mao and S. Zhang, *Biomacromolecules*, 2015, **16**, 1987–1996.
15 W. X. He, A. K. Rajasekharan, A. R. Tehrani-Bagha and M. Andersson, *Adv. Mater.*, 2015, **27**, 2260–2264.
16 H. P. Schwarcz, E. A. McNally and G. A. Botton, *J. Struct. Biol.*, 2014, **188**, 240–248.
17 J. Mahamid, A. Sharir, L. Addadi and S. Weiner, *Proc. Natl. Acad. Sci. U. S. A.*, 2008, **105**, 12748–12753.
18 S. Weiner, I. Sagi and L. Addadi, *Science*, 2005, **309**, 1027–1028.
19 H. Zhang, Q. W. Fu, T. W. Sun, F. Chen, C. Qi, J. Wu, Z. Y. Cai, Q. R. Qian and Y. J. Zhu, *Colloids Surf., B*, 2015, **136**, 27–36.
20 R. Zhou, W. Xu, F. Chen, C. Qi, B. Q. Lu, H. Zhang, J. Wu, Q. R. Qian and Y. J. Zhu, *Colloids Surf., B*, 2014, **123**, 236–245.
21 J. L. Min, J. B. Park, H. H. Kim, S. K. Chang, S. Y. Park, H. J. Kim and H. P. Young, *Macromol. Res.*, 2014, **22**, 710–716.
22 F. Zhang, X. You, H. Dou, Z. Liu, B. Zuo and X. Zhang, *ACS Appl. Mater. Interfaces*, 2015, **7**, 3352–3361.
23 S. Jiang, H. Pan, Y. Chen, X. Xu and R. Tang, *Faraday Discuss.*, 2015, **179**, 451–461.
24 Y. Seo, T. Goto, S. Cho and T. Sekino, *Materials*, 2020, **13**, 3281.
25 M. A. Koperska, D. Pawcenis, J. Bagniuk, M. M. Zaitz, M. Missori, T. Łojewski and J. Łojewska, *Polym. Degrad. Stab.*, 2014, **105**, 185–196.

26 X. L. Ma, R. Li, L. Ru, G. W. Xu and Y. P. Huang, *eXPRESS Polym. Lett.*, 2010, **4**, 321–327.
27 R. Kino, T. Ikoma, A. Monkawa, S. Yunoki, M. Munekata, J. Tanaka and T. Asakura, *J. Appl. Polym. Sci.*, 2006, **99**, 2822–2830.
28 X. Hu, W. Zhang and D. Hou, *Ceram. Int.*, 2020, **46**, 9810–9816.
29 P. Hang, X. Hao, B. L. Su, Y. B. Cheng and Z. Fu, *J. Mater. Chem. B*, 2015, **3**, 4496–4502.
30 T. Tsuchida, J. Kubo, T. Yoshioka, S. Sakuma, T. Takeguchi and W. Ueda, *J. Catal.*, 2008, **259**(2), 183–189.
31 B. Marelli, C. E. Ghezzi, A. Alessandrino, J. E. Barralet, G. Freddi and S. N. Nazhat, *Biomaterials*, 2012, **33**, 102–108.
32 J. Wang, Q. Yang, C. Mao and S. Zhang, *J. Biomed. Mater. Res., Part A*, 2012, **100**, 2929–2938.
33 H. Liu, J. Cheng, F. Chen, F. Hou, D. Bai, P. Xi, Z. Zeng, H. Liu, J. Cheng and F. Chen, *ACS Appl. Mater. Interfaces*, 2014, **6**, 3132.